Proceedings of the 12th International Conference on
Aluminium Alloys, September 5-9, 2010, Yokohama, Japan
©2010 The Japan Institute of Light Metals
pp. 528-535

Microstructurally Based Models for Shear Localization and Formability in Automotive Aluminum Alloys

Xiaohua Hu[1], David S. Wilkinson[1], Mukesh Jain[1], Jidong Kang[1], Raja K. Mishra[2]
[1] Department of Materials Science and Engineering, McMaster Centre for Automotive Materials, McMaster University, Hamilton, Ontario L8S 4L7, Canada
[2] General Motors Research and Development Center, Warren, MI 48090-9055, USA

The drive to reduce the weight of vehicle structures has provided a great deal of impetus for the development of cost-effective processing routes that can be used to make high quality components for chassis and closure applications from aluminum alloy sheet. With this comes the need to develop models for fabrication processes such as stamping and hemming that can deal with these complex materials. While empirically derived constitutive laws can be used in many cases, one would prefer to use models that have the key features of the microstructure built in. For the past few years we have been working towards such models, primarily in Al alloys. In this paper an overview is presented on the role of second phase particles on processes that control ductility such as shear localization and damage. In particular, the effect of microstructure on the formability of the AA5754 aluminum alloy is studied in conventional DC cast alloys and continuous cast (CC) alloys made by twin belt casting. Here Fe-based intermetallic particles, distributed both as isolated particles and in stringers, contribute to early shear localization, thus limiting the formability of sheet metals during forming. A novel two-stage modeling procedure is developed to study the influences of particles distributions on pre-necking and post-necking behaviors during uniaxial tension. Macro-micro multi-scale models are developed for complex forming processes, where the microstructures such as particles and grain structure can be incorporated in the micro-level models. The macro-micro approach has been applied to study the influence of the second phase hard particles on wrap bendability.

Keywords: *formability, aluminum alloys, strain localization, fracture, bendability, multi-scale modeling.*

1. Introduction

It is important to understand and predict the localization behavior and damage for the development of high formability materials, especially for lightweight automotive aluminum sheets capable of replacing steel sheets in automobiles for mass reduction and environmental benefits. The aluminum sheets produced by the conventional direct chill cast (DC) technology (hereafter called DC alloy) is costly. The continuous strip casting (CC) technology (hereafter called CC) has received interest because of the considerable cost reduction. The mechanical tests of AA5754 aluminum sheets by uniaxial tension have shown that the CC and DC alloys have similar formability in terms of localized necking strain. The CC sheets, however, tend to exhibit much less post-localization deformation and lower fracture strains compared to DC sheets during uniaxial tension. The formability of materials, as well as localization and post-localization behavior is related to the material's constitutive law, including work hardening/softening behavior [1] and the strain rate sensitivity. Moreover, it depends also on microstructural inhomogeneities in the alloy. The influence of the constitutive law and microstructural inhomogeneities, however, depend upon the geometric effect (also called geometric softening) [2] and the specific loading conditions. Based on the deformation sequences during uniaxial tension, we have developed a two stage, two dimensional (2D) finite element (FE) analysis [3] corresponding to pre-necking and post-necking stages of deformation.

Currently, aluminum alloy sheets with good bendability are strongly desired in the automotive industry for forming complex shapes with small bend radii. Good bendability is strongly desirable for continuously cast (CC) aluminum sheet due to its lower cost of production. As for automotive aluminum alloys , e.g. AA5754 and AA6111, bendability has been shown by some experiments such as V-bend and Wrap-bend tests to be strongly correlated with the material microstructures, especially, the statistics of second phase particles such as volume fractions and distributions [4]. Computational modeling, e.g., finite element (FE) analysis, is still lacking for explicitly verifying these experimental results as well as in predicting the bendability of materials with different microstructures. Such studies will pave the way for the microstructurally design for good bendability. As discussed in a paper describing simulations of the uniaxial tension tests [3], it is impractical to consider a full 3D sample sized, microstructure-based, FE model with realistic microstructure inputs for forming simulations. However, a plane strain condition, except for the edge regions, can be assumed for bending of sheets by considering the strain in the transverse direction (TD) to be zero. The bending operations are rather complex where contacts between tools and materials are involved and the deformation is quite inhomogeneous in different sections of the bend. The complexity, however, can be adequately dealt with by a macro-micro multi-scale finite element modeling procedures. Firstly, a sample sized plane strain macro model simulation for wrap-bending is performed and the location of most severe deformation is identified. Then a microstructurally based sub-model (plane strain) of this location is developed and simulation is performed with microstructural inputs such as second phase particles and grain structures. The displacement history of the region is taken from the macro model and applied as a boundary condition in the micro model.

In the following, the above mentioned methodologies and their applications will be explained in more details. It must be noted the current paper is a review of published papers [3,5,6,7]. Readers are encouraged to read those papers for more details.

2. The two-stage modeling procedure

2.1 The methodology

For a sheet sample undergoing uniaxial tension, localized deformation is expected to develop, wherein the strain eventually becomes concentrated in a shear band leading to fracture (see Fig. 1 (a)). Localized deformation starts with diffuse necking. For sheet samples the length of the diffuse necking region is comparable to the width (w) of the sample. As deformation proceeds further, a localized necking band develops within the diffuse necking region, the width of which is comparable to the thickness of the sample (t). Further deformation is then confined within this band until the final failure occurs. Deformation in the necking band is believed to be in plane strain, where the strain associated with the direction of the band is zero and that outside the band is very small compared to that in the band itself. This paper deals with finite element modeling of strain localization based on microstructural characteristics. Firstly, we utilize a plane stress unit-cell model to study the behavior from uniform deformation to the onset of localized necking [3,8]. Some parametric studies are performed with models containing only two particles [8] and subsequently, the measured particle fields of CC and DC are also considered [3]. The particles are embedded in either a homogeneous or an inhomogeneous matrix. The modeling plane of the plane stress analysis is RD×TD, as shown in Fig. 1, where the stress associated with the ND direction is zero (RD, TD and ND stand for rolling, transverse and the normal directions, respectively). Uniaxial tension is applied parallel to RD. The top and bottom edges are constrained by an EQUATION type multipoint constraint (MPC) to ensure that edges remain straight during deformation. This condition will prevent the width instability, and therefore diffuse necking. The matrix is treated as an isotropic material in the continuum sense and the inhomogeneity is introduced by a spatial grain orientation distribution, where each grain possesses a different strength in terms of its Taylor factor, which is assumed to remain constant during deformation. User material models are employed to represent this constitutive behavior.

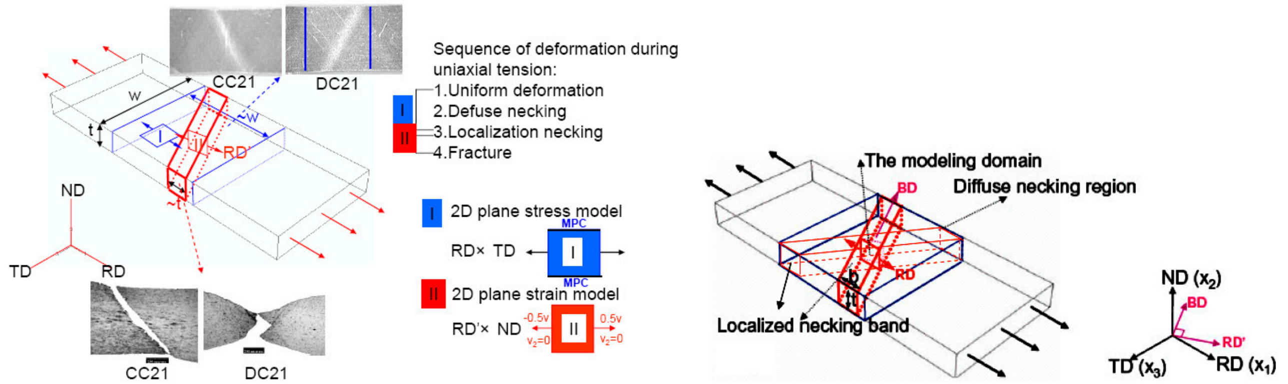

(a) (b)

Fig. 1. (a) The sequence of localized deformation during uniaxial tension [3]. (b) A sketch showing the modeling domain of the modified edge constrained plane strain post-necking model

Once localized necking starts, deformation becomes plane strain within the localization bands, where the strain associated with the direction of the band (BD) is zero and strain outside the band is small. Thus a plane strain model is useful to understand the behavior from the onset of localized necking to fracture [3]. The domain of validity of the plane strain model is inside the band cross section (RD'×ND), where RD' is perpendicular to the BD×ND plane as shown in Fig. 1(b). Only the inhomogeneity caused by particles is considered in the plane strain model. The deformation is applied to the left and right edges in the loading direction (RD'), but fixed in the normal direction (ND), while the top and bottom edges are free to deform in both degrees of freedom of the simulation plane. Shear type failure model with a local fracture strain criterion is applied to both particles and the matrix material, while tension failure model with a tensile hydrostatic stress criterion is applied to the particles. The post-necking model domain (RD'×ND) proposed in [3] was later modified to the RD×ND cross section and reasons are detailed by Hu et al. in [5,6].

2.2 Results and discussion

2.2.1 Plane stress models

With the two particle-model [8], the alignment and interparticle spacing are varied. Then grain structures are introduced in the model. Meshing sensitivity and the effects of mesh homogeneity have been discussed in details elsewhere. The grain structures have been introduced by the use of a user material subroutine based on pre-generated mesh, resulting in ragged grain boundaries [8]. It is concluded that a homogeneous mesh is essential to have sound prediction and good comparability between models. The results show that the models are more prone to localization when the two particles are aligned along the loading direction or close-packed [8]. All the results show that the location of shear band formation and value of localization strain are insensitive to that of particles and they are mainly determined by the arrangement of soft grains. The localization strain is slightly decreased if the two particles straddle the shear band. The conclusion of relative effect of grain structures and particles is valid for larger scale models when measured particle field and grains are mapped into the plane stress models [3].

2.2.2 Plane strain models

Due to rather fine finite element meshes with mesh size of 0.238 μm which directly represent the pixel map of optical metallographs, we were only able to consider very small particle fields of 0.071×0.095 mm^2 in the post-necking models with rather limited number of particles in the models which may not be representative of the particle distributions of the whole material [3]. Few statistical parameters can be extracted from these models to study the influence of these parameters on post-necking deformation and failure mode. In a later parametric study, a simplified large-scale model was considered with homogeneous meshes which contains equal sized particles shaped as squares with each square represented by one-single element [6]. With this simplified representation of particles, we were able to perform a comprehensive parameter study for a virtual large particle field where the influences of total particle volume fraction, stringer volume fraction, stringer length, inter-particle spacing in stringers and model thickness etc. on post-necking and fracture topography are studied. The dimension of the models, e.g., the thickness range of t_0=0.43-0.86 mm which corresponds to the initial thickness of t_i=0.5-1 mm before uniaxial tension deformation, is large and comparable to actual samples. The number of particles considered is in the order of several thousands, and therefore one can generate statistically representative distribution of stringers or isolated particles. The modeling results indicate that the post-necking behavior of alloys with a ductile matrix is not controlled by a single particle or a pair although they may become sites for initiation of damage. On the other hand, the distribution of the particle field in the material is important for the total deformation behavior. Multiple damage sources such as stringers can act cooperatively and speed up the damage process in the material, thereby producing smaller post-necking deformation. The particle distribution is, however, a very complex problem with many parameters needed to fully describe it. We have studied five parameters in the models and all have significant influences on post-necking deformation. Post-necking deformation decreases with increasing total particle volume fraction (f_p) and stringer fraction (f_s) and model dimensions, but increases with inter-particle spacing R.

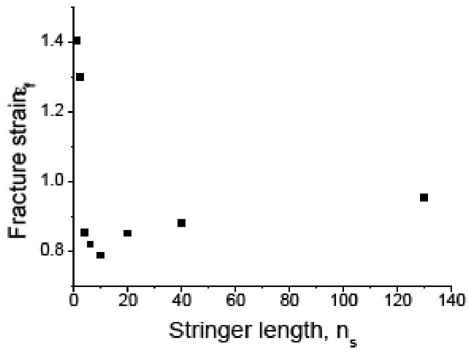

Fig. 2. The influence of stringer length on the macroscopic fracture strains.

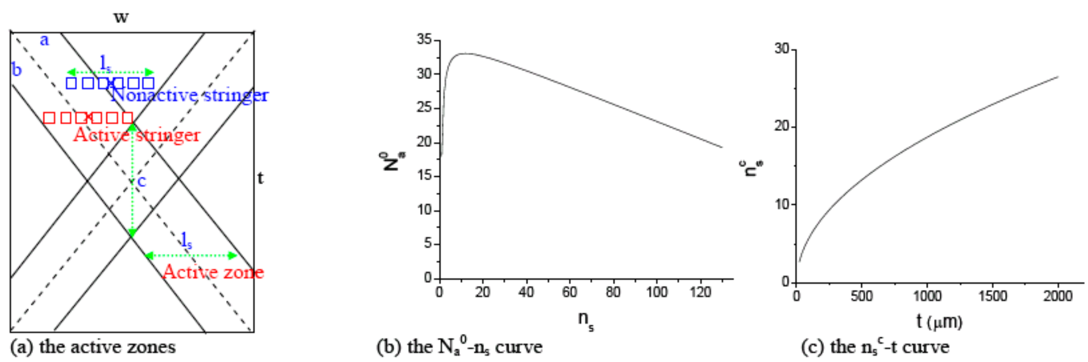

Fig. 3. (a) A sketch showing the active zones (AZ) and non active zones (NA) where a stringer of length l_s is seen as active when its center (denoted by x in the sketch) lies within AZ (e.g. the red one) which has a lateral width of l_s, and inactive when it lies within NA (e.g. the blue one), (b) The relationship between N_a^0 and n_s and (c) The relationship between the critical stringer length n_s^c and model size.

The influence of stringer length (n_s), however, is different, in that the fracture strain decreases sharply with increasing stringer length and reaches a minimum for n_s=10. The observation suggests that the post-necking deformation is inversely related to the number of active damage sources (N_a) which lie within the damage path. The initial number of active damage sources (N_a^0) can be estimated if we randomly assign the positions of single particles and stringers in the model. A stringer is thought to be initially active when any one particle in the stringer or the gap between any two particles straddles the diagonals of the model (the black dashed line in Fig. 3(a)). A detailed analytical procedure to calculate N_a^0 has been explained in detail by Hu et al. [6] and its relationship with stringer length is shown in Fig. 3(b). The critical value (N_s^c) of N_a^0 correlates well with finite element calculation and it also depends on the sample dimension (see Fig. 3(c)).

3. The macro-micro multi-scale approach for studying wrap-bending

3.1 Methodology

The multi-scale procedure for a wrap bending model is shown schematically in Fig. 4. The global plane strain model has a sheet thickness *t* of 1 mm and a length of 18 mm. With both a roller and a mandrel in contact with the sheet, the bending deformation is applied by rotating the roller by 180° around the center of the mandrel while keeping the left edge of the sheet fixed. In the example shown in Fig. 4, the radius of the roller and the mandrel are 2 mm and 0.25 mm respectively. For the global model, the entire sheet specimen is meshed with linear rectangular plane strain elements with reduced integration (4PE4R) in ABAQUS/Explicit [9]. Only the section of 3 mm sheet length (Fig. 4(c)) where the roller will roll over will undergo noticeable large deformation during deformation. Therefore, a fine mesh of 20×20 μm^2 sized squares is utilized, while the rest of the specimen is represented by a coarser mesh. At the end of deformation, the equivalent strain contours are drawn and the positions of bending zone with largest deformation are identified. Subsequently, a 1.0×0.4 mm^2 area sub model with 1 μm^2 mesh size for incorporating the particle field and grain structure data is chosen for simulation. The internal edges of the sub-models in Fig. 1(d), i.e., the vertical edges (a and c) and bottom edge b, are driven by the displacement history of the edges determined from the global model. The edge d (see Fig. 8 (b) and (d)) represents the top surface that is free to deform except the contacts with the roller which is made to roll over it as in the global model.

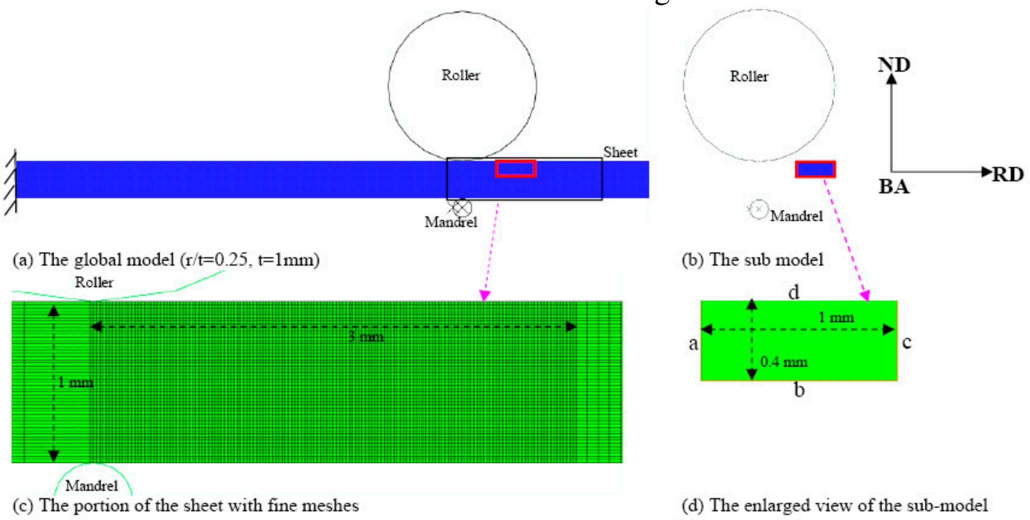

Fig. 4. The multi-scale scheme for wrap bending.

3.2 Results and discussions

3.2.1 The global model and the regions of most severe deformations

Two mandrel radii *r* of 0.25 mm and 0.5 mm, corresponding to *r/t*=0.25 and 0.5 respectively with a sheet thickness of t=1 mm are chosen while keeping the other geometric parameters the same. The equivalent strain contours at final deformation for the two models with different mandrel radii are shown in Fig. 5(a) and (b). As expected, there are two regions of large deformation where the sheet is bent over the mandrel, which are at the outer (top) and inner (bottom) surfaces. The outer surface experiences hydrostatic tensile stresses which usually causes material damage, while the hydrostatic stresses on the inner surface are compressive. Therefore, the region at the outer surface is of interest in the current study, due to fact that it is the preferential site for crack initiation.

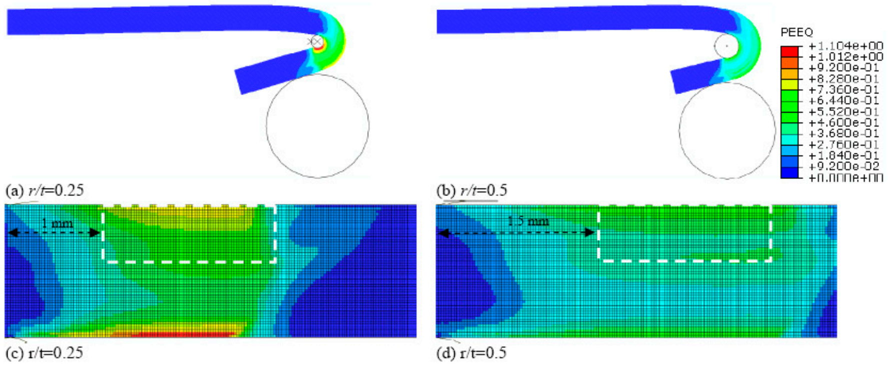

Fig. 5. The equivalent strain contours plotted on (a) and (b) deformed, (c) and (d) the non-deformed shapes where the regions of most severe deformations are delineated by white dashed line rectangles for sub-models.

To determine the region for use in the sub-model, the equivalent strain contours in Fig. 5(a)-(b) are re-plotted on non-deformed model geometries in Fig 5(c)-(d) to determine precisely the location of the most severe deformation region in the original configuration. It can be seen from the figure that the spread of strain distribution of the bending zone is larger when the radius changes from 0.25 mm (Fig. 5(c)) to 0.5 mm (Fig. 5(d)). The strain is more concentrated and a higher maximum local strain is induced when the bending radius, i.e., the radius of the mandrel, is smaller, which can lead to earlier failure. The minimum ratio between bending radius and sheet thickness (r/t) free of specimen cracking is usually taken as a measure of the bendability of sheet materials [10,11]. Likewise, the material that has smallest angle of bending before apparent cracking exhibits the poorest bendability for the same r/t value. From Figs. 5(c)-(d), the top-left corner of the sub-model (refer to the white frames in the figures) is determined to have a distance of 1 mm away from the initial point of contact between the roller and the sheet when r=0.25 mm.

3.2.2 The sub-models

In the initial stages, the sub-models consider only the microstructural inhomogeneities due to second phase hard particles and their distributions, while the matrix material is assumed to be homogeneous. As stated previously [3,5], the use of actual measured particle field such as by direct pixel mapping will need a very fine mesh and to build such a model at the scale of millimeter sample thickness will require a large number of elements and make the model computationally unmanageable. Simplification of particles as ellipses, meshed in ABAQUS/CAE pre-processor, will generate an inhomogeneous mesh that has proven to give inconsistent simulations results. A complete homogeneous mesh is adopted. Simplified virtual particle fields are generated, where each particle is identical in size with a square shape represented by one single element. The virtual particle fields over the sub-model domain of 0.4×1 mm^2 are created by randomly positioning isolated particles in the models of 400×1000 ABAQUS equal-sized (1 μm), linear plane strain square elements. In this work, each stringer consists of 10 particles and the ligament spacing between particles is chosen to be 1 μm, i.e., one element apart. Apart from the models of 100% random distributions and 100% stringer distributions of particles, models of intermediate distributions are also considered. The models of intermediate distributions consist of 20%, 40%, 60%, 80% stringers with the rest being random particles. The total volume fraction of particles in all the models is kept constant at 2%, based on experimental data of AA5754 alloys with 0.21 wt % Fe content.

Equivalent plastic strain contours were obtained at the end of simulations of the microstructure-based sub-models with the bend angle (α) of 180^o for both 100% random and 100% stringer particle distributions respectively for a r/t ratios of 0.5, i.e. r=0.5 mm, No apparent damage is seen in the model with a 100% random distribution. There is an observable local damage at the surface for the model with a 100% stringer distribution. This damage, however, does not propagate through the thickness to form macroscopic cracks. From the equivalent plastic strain maps of models with different stringer levels from 0% to 100% stringers for r/t=0.25, no apparent damage develops when the model consists of 100% random particles. When the model has 100% stringer, however, there is observable damage on the surface at a bend angle of $\alpha=100^{o}$. With continued deformation, considerable damage can be observed leading to very large cracking at $\alpha=180^{o}$. For the models of intermediate particle distributions, in general, the extent of crack opening is proportional to the volume fraction of stringers. For the case of 20% stringers, a crack developed just beneath the surface and a shear band leading up to the surface developed from the crack. When the volume fraction of stringers is increased to 40 %, multiple crack openings are found. None of these cracks, however, propagates deep through the thickness. With stringer volume fraction greater than 60%, however, a large crack can be developed along with several minor surface cracks. The crack initiation is closely related to the local particle distributions near the surface, while the crack propagation is related to the particle distribution underneath this location.

To illustrate the details of particle distributions on crack initiation and propagation, the crack paths are shown on the equivalent strain contours drawn on the non-deformed shape in Figs. 6(a)-(d) for various bend angles and 100% stringer particle distribution. In these figures, the areas delineated by rectangles are enlarged to show the details of the crack propagation paths. The damage is initiated close to the surface near or between particles in stringers (Fig. 6(a)) where the stringers are more densely packed. The damage propagates towards other area with densely packed stringers (Fig. 6(b)) through localized shear bands. The crack propagation through the thickness occurs along stringers and jumps in a zig-zag manner to other stringers (Fig. 6(c)) through excessive deformation of the shear bands in the matrix material. Another interesting phenomenon is that the shape of crack path is curved where the path is more parallel to the sample surface when it propagates through the thickness, which is consistent with experimental observation, which can facilitate crack propagation along the stringer when the crack goes deep. It must be noted that the propagating crack at the very end of the simulation may not be real as it is too close to the bottom edge where displacement is driven by the results from the global model where a more gradual and homogeneous deformation is enforced even if the inhomogeneity due to particle distributions is introduced there (Fig. 10(d)).

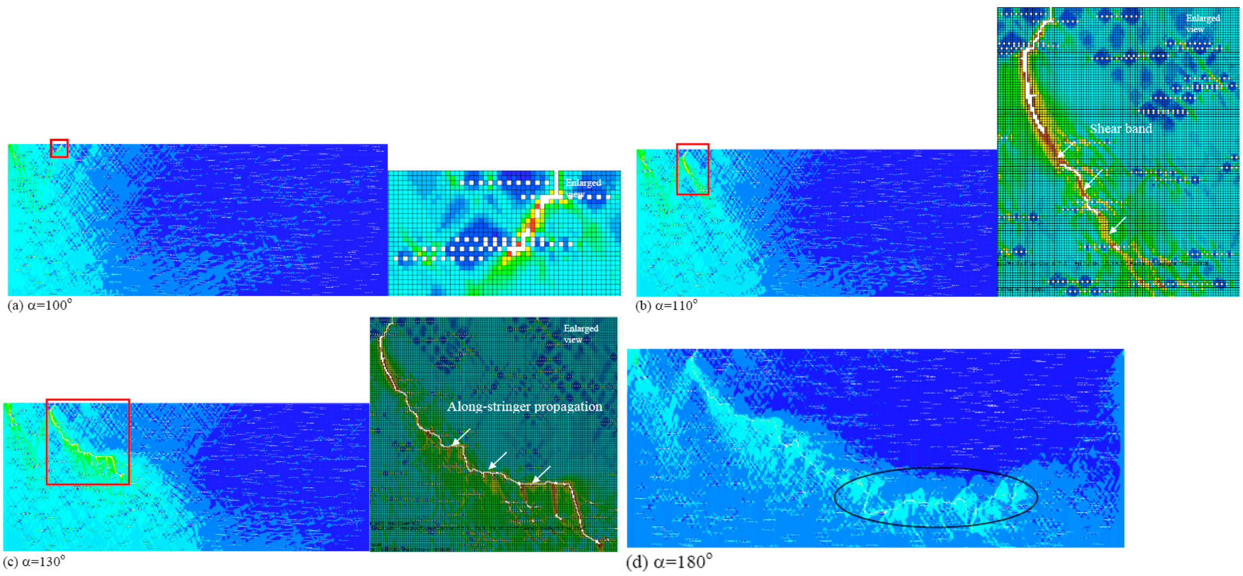

Fig. 6. The equivalent strain contours drawn on non-deformed shape which shows the damage evolution with bending angles for the sub-models for the case of 100% stringer and r/t=0.25

As for the influence of stringer volume fraction, the observation can be explained as follows. The higher the volume fraction, the smaller is the average spacing between stringer through the thickness and consequently, there are more areas of densely packed stringers. These densely packed stringer regions facilitate faster crack propagation and lead to larger cracks at the end of deformation. However, it seems that there is an exception (scatter) for the case when the stringer fraction is 60%, where longer and larger cracks are developed than the case when the fraction is 80 %. In this case the initial and lone large crack is propagated through the thickness until the final deformation. It is to be expected that there is some scatter in the results because random positioning of the isolated particles or stringer in the virtual particle field generation process may not be completely "random". The fields generated from different randomization attempts are actually not the same. In this particular case, the arrangement of stringers on the left side of the model on the surface and underneath facilitates the propagation of the initial nucleated crack. It seems that the cracks initiated earlier will be long and wide toward the end as they endure longer propagation times than those initiated later.

4. Conclusion

From this review of microstructure-based models of formability of automotive aluminum alloys, it is seen that the inhomogeneity caused by spatial grain orientation distributions and second phase hard particles have important roles in the development of strain localization. The particle distribution plays a key role in controlling the fracture process such as post-necking deformation and fracture in uniaxial tension and the bending behavior in wrap bending tests. In agreement with experimental observations, the models indicate that stringer distribution will shorten the post-necking thinning process and lead to earlier fracture and inferior bendability.

References

[1] Hu, X. H., Gasperini, M., and Van Houtte, P., Materials Science Forum 2005;495-497:1103.
[2] Tvergaard, V., Computer Methods in Applied Mechanics and Engineering 1993;103:273.
[3] Hu, X. H., Jain, M., Wilkinson, D. S., and Mishra, R. K., Acta Materialia 2008;56:3187.
[4] Sarkar, J., Kutty, T. R. G., Conlon, K. T., Wilkinson, D. S., Embury, J. D., and Lloyd, D. J., Materials Science and Engineering A 2001;316:52.
[5] Hu, X. H., Wilkinson, D. S., Jain, M., and Mishra, R. K., International Journal of Solids and Structures 2009;46:2650.
[6] Hu, X. H., Wilkinson, D. S., Jain, M., and Mishra, R. K., International Journal of Fracture 2010;164:167.
[7] Hu, X. H., Wilkinson, D. S., Jain, M., Wu, P. D., and Mishra, R. K., Journal of Materials Processing Technology 2010;210:1232.
[8] Hu, X. H., Wilkinson, D. S., Jain, M., and Mishra, R. K., Modelling and Simulation in Materials Science and Engineering 2007;15:893.
[9] ABAQUS Inc., ABAQUS Mannual Version 6-5.1, 2006.
[10] Datsko, J and Yang, C. T., Journal of Engineering for Industry 1960;82:309.
[11] Carsley, J. and Kim, S., Journal of Materials Engineering and Performance 2007;16:331.